Hindawi Publishing Corporation
EURASIP Journal on Advances in Signal Processing
Volume 2008, Article ID 756414, 15 pages
doi:10.1155/2008/756414

Research Article

Low Complexity Track Initialization from a Small Set of Non-Invertible Measurements

Christian R. Berger,[1] Martina Daun,[2] and Wolfgang Koch[2]

[1] *Department of Electrical and Computer Engineering, University of Connecticut, 371 Fairfield Way U-2157, Storrs, CT 06269, USA*
[2] *Sensor Networks and Data Fusion Group, FGAN e.V., Neuenahrer Strasse 20, 53343 Wachtberg, Germany*

Correspondence should be addressed to Christian R. Berger, crberger@engr.uconn.edu

Received 30 March 2007; Accepted 15 November 2007

Recommended by T. Luginbuhl

Target tracking from non-invertible measurement sets, for example, incomplete spherical coordinates measured by asynchronous sensors in a sensor network, is a task of data fusion present in a lot of applications. Difficulties in tracking using extended Kalman filters lead to unstable behavior, mainly caused by poor initialization. Instead of using high complexity numerical batch-estimators, we offer an analytical approach to initialize the filter from a minimum number of observations. This directly pertains to multihypothesis tracking (MHT), where in the presence of clutter and/or multiple targets (i) low complexity algorithms are desirable and (ii) using a small set of measurements avoids the combinatorial explosion. Our approach uses no numerical optimization, simply evaluating several equations to find the state estimates. This is possible since we avoid an over-determined setup by initializing only from the minimum necessary subset of measurements. Loss in accuracy is minimized by choosing the best subset using an optimality criterion and incorporating the leftover measurements afterwards. Additionally, we provide the possibility to estimate only sub-sets of parameters, and to reliably model the resulting added uncertainties by the covariance matrix. We compare two different implementations, differing in the approximation of the posterior: linearizing the measurement equation as in the extended Kalman filter (EKF) or employing the unscented transform (UT). The approach will be studied in two practical examples: 3D track initialization using bearingsonly measurements or using slant-range and azimuth only.

1. INTRODUCTION

Target tracking from incomplete polar or spherical measurements, like bearings only or range only, is a topic that has received close investigation, for example, target motion analysis and related questions of observability [1, 2]. The results utilize derivatives of standard extended Kalman filters, typical of tracking targets using measurements in polar or spherical coordinates, while modeling their movement in Cartesian coordinates (see [3–5] and references therein).

In the case of incomplete polar or spherical measurements, the full target state vector is not directly observable, since we cannot invert the measurement function. This makes the initialization of the extended Kalman filter with an initial state estimate and corresponding covariance crucial for its performance, otherwise the filter can easily become unstable [6]. In our case, this cannot be accomplished by direct inversion of the measurement function. A set of multiple measurements must be combined for initialization, which calls for a sensible data fusion. Typically, numerical batch estimators are used to find a maximum likelihood (ML) estimate [7]. Although these estimators offer close-to-optimal performance, in the sense of achieving the Cramér-Rao lower bound (CRLB) in estimation accuracy, they need a large number of measurements for "benign" numerical behavior, that is, with few, possibly asynchronous measurements, convergence will be very slow. We offer instead an analytical approach using a small or minimum set of measurements, to return an initial estimate and a corresponding covariance.

Our goal will be to initialize the target state from a small or minimum set of measurements using a low-complexity algorithm. These two objectives are very important, for example, when using a multihypothesis tracker (MHT) in a realistic environment, featuring clutter and/or multiple targets [8]. Initializing from a large set of measurement cycles becomes prohibitively complex, as the number of possible

combinations quickly becomes too large to handle. In any case, the complexity per calculation should be small, as still many evaluations will be necessary due to clutter and/or multiple targets.

To be able to analytically invert the nonlinear measurement equations, we adopt two methods: (i) to avoid an underdetermined equation system we initialize some state vector components using statistical assumptions; and (ii) to avoid an overdetermined equation system we first initialize from a subset of measurements only, incorporating leftover measurements afterwards, simply using Kalman filter iterations.

By making statistical assumptions about some components of the state vector, we can initialize these state elements with their mean and covariance, and thereby find an initial estimate even in cases when the full-state vector is statistically unobservable. When splitting the state vector into two parts, one of which is estimated and the second initialized through statistical assumptions, the covariance of the latter is a design choice, but we will still have to derive the cross-correlation between the two. More importantly, the added uncertainty in the covariance of the estimated parameters must be modeled. This is caused by the loss of information due to not estimating part of the state vector and instead interpreting this as an additional perturbation.

Initializing only from a subset of measurements and utilizing leftover measurements in a following (extended) Kalman filter iteration is suboptimal in the nonlinear case, but greatly reduces complexity. By avoiding an overdetermined equation system, in most cases we will find a straightforward analytical solution. Cases of no solution or ambiguities can be overcome using the leftover measurements: choosing a different subset in the case of no solution or using a simple likelihood test on the leftover measurements to choose one of ambiguous solutions. Additionally, we will minimize the loss of initialization accuracy by choosing the best subset of measurements, using a suitable optimality criterion, for example, the trace of the estimated covariance matrix.

After deriving a general approach, we will apply it to different scenarios, mostly using incomplete spherical measurements typical for radar/sonar applications. Special focus will be on position initialization from bearings-only measurements (Section 3), also treated in [5], which this work was strongly inspired by. As an additional application scenario, we will present position initialization from two slant-range and azimuth measurements.

Last, all scenarios are numerically evaluated via Monte Carlo simulation. Focus will be on absolute performance like estimation error and comparisons to the corresponding CRLBs. Consistency of our initialization will be scrutinized to check if our estimators are unbiased and if the covariance precisely characterizes the estimation error.

This work has the following structure: after this introduction, we will describe the system model and derive our initialization scheme in Section 2. As mentioned before, Section 3 will cover the bearings-only scenario, which is followed by the scenario of range and azimuth (Section 4). We will discuss our numerical simulations in Sections 5 and 6 concludes this report.

We would like to adopt the following notation: vectors are represented by bold lowercase letters, while matrices can be represented by both bold and regular uppercase letters. The notation A' denotes the transpose of matrix A. The concatenation of two functions f and g, where $f : \mathbb{R}^m \to \mathbb{R}^n$ and $g : \mathbb{R}^n \to \mathbb{R}^p$, is expressed as $g \circ f : \mathbb{R}^m \to \mathbb{R}^p$.

2. DESCRIPTION OF SYSTEM MODEL AND MAP ESTIMATION

2.1. System model

Let $\mathbf{x}$ be the state vector of the target with dimension $\eta_{\mathbf{x}}$, which is modeled in Cartesian coordinates using, for example, a second-order motion model

$$\begin{aligned} \mathbf{x}(n+1) &= F(n)\mathbf{x}(n) + \nu(n), \\ \mathbf{x} = \begin{pmatrix} \mathbf{p} \\ \mathbf{v} \end{pmatrix}, \quad F(n) &= \begin{pmatrix} I & t_{n+1} - t_n \\ 0 & I \end{pmatrix} \end{aligned} \tag{1}$$

with $\mathbf{x}$ being the state vector, containing position vector $\mathbf{p}$ and velocity vector $\mathbf{v}$, ν the process noise, and F the state propagation matrix, all of dimension $\eta_{\mathbf{x}}$. The measurement function h is generally nonlinear, dependent on the state vector of the observer $\mathbf{x}_s$ and not invertible,

$$\mathbf{z}(n) = h(\mathbf{x}(n), \mathbf{x}_s(n)) + \mathbf{w}(n), \tag{2}$$

where we will omit the dependency of h on $\mathbf{x}_s$ in the following to shorten notation. The zero-mean, Gaussian measurement noise $\mathbf{w}$ and the observation $\mathbf{z} \in M$ (M is the space of the measurements) are of dimension $\eta_{\mathbf{z}}$.

To formally divide the state vector $\mathbf{x}$ into a part which is estimated and one which we initialize using statistical assumptions, we introduce two matrices:

$$\mathbf{x} = K\mathbf{p} + \overline{K}\mathbf{v} \quad \text{with } K = \begin{bmatrix} I \\ 0 \end{bmatrix}, \overline{K} = \begin{bmatrix} 0 \\ I \end{bmatrix}. \tag{3}$$

Remark 1. In our applications, we will initialize the position $\mathbf{p}$ and make statistical assumptions about the velocity $\mathbf{v}$, to overcome the asynchronicity between measurements. This can easily be generalized to any division into subvectors, reordering them to achieve the same format as in our derivation.

2.2. Underdetermined equations

Combining k different measurements and our statistical assumptions, we try to find an estimator t with $t : M^k \to \mathbb{R}^{\eta_{\mathbf{p}}}$ which fulfills the following condition:

$$t \circ h(K\mathbf{p} + \overline{K}E[\mathbf{v}]) = \mathbf{p}, \tag{4}$$

that is, if our assumptions on $\mathbf{v}$ hold, then t gives the correct value $\mathbf{p}$. In the case of linear functions, this would be equivalent to an unbiased estimator. We have to combine at least

k measurements so that $k\eta_{\mathbf{z}} \geq \eta_{\mathbf{p}}$. To simplify notation, we will use $t(\mathbf{z})$ also when referring to $t(\mathbf{z}^k)$ and use $h(\mathbf{x})$ even for mapping to $\mathbf{z}^k$. Since the function t is generally not readily available, defining it in a sensible way will be one of the main tasks of this work.

2.3. Overdetermined equations

Generally if we have $k\eta_{\mathbf{z}} > \eta_{\mathbf{p}}$, there is no solution to the overdetermined equation $\mathbf{z} = h(K\mathbf{p} + \overline{K}\mathbf{v})$ due to the measurement errors. Instead of picking a $\mathbf{p}$ which reproduces all measurements as closely as possible in the ML sense, we drop n arbitrary parts of the measurement to achieve a well-determined equation, that is, $k\eta_{\mathbf{z}} - n = \eta_{\mathbf{p}}$. Even though we are faced with nonlinear equations, this will lead to a well-defined solution in most cases.

By systematically dropping different parts of the measurements we produce several, $\binom{k\eta_{\mathbf{z}}}{n}$, estimates and pick one using an optimality criterion, for example, the trace of the estimated covariance matrix. If one combination of measurements renders no solution, it is excluded. Combinations of measurements leading to ambiguous solutions utilize the left overmeasurements in a simple likelihood test to overcome the ambiguity (for an explicit example see Section 3.2.2).

Afterwards, each of the n remaining measurements is merged using Kalman filter iterations, which, if the problem was purely linear Gaussian, would return the same final result for any initial combination of measurements. Since our problem is inherently nonlinear, this way we initialize from the measurements with the best geometry.

2.4. MAP estimate using extended kalman filter linearization

Let the likelihood function $p(\mathbf{z} \mid \mathbf{x})$ be given by a Gaussian distribution $\mathcal{N}(\mathbf{z}; h(\mathbf{x}), \mathbf{R})$, with a known measurement covariance matrix $\mathbf{R}$. The probability density of $t(\mathbf{z})$ given $\mathbf{x}$ can be approximated by linearizing $t(\mathbf{z})$:

$$p(t(\mathbf{z}) \mid \mathbf{x}) \cong \mathcal{N}\left(t(\mathbf{z}); t[h(\mathbf{x})], \frac{\partial t}{\partial \mathbf{z}}\mathbf{R}\frac{\partial t'}{\partial \mathbf{z}}\right). \tag{5}$$

Looking at (4), we can easily see that by definition $t \circ h$ can be linearized around $E[\mathbf{v}]$ to

$$t \circ h(\mathbf{x}) \cong \mathbf{p} + \frac{\partial(t \circ h)}{\partial \mathbf{v}}(\mathbf{v} - E[\mathbf{v}]). \tag{6}$$

For brevity of notation we define $G = \partial(t \circ h)/\partial \mathbf{v}$, with this we have

$$ep(t(\mathbf{z}) \mid \mathbf{x}) \cong \mathcal{N}\left(t(\mathbf{z}); \mathbf{p} + G(\mathbf{v} - E[\mathbf{v}]), \frac{\partial t}{\partial \mathbf{z}}\mathbf{R}\frac{\partial t'}{\partial \mathbf{z}}\right) \tag{7}$$

and due to linearization we can switch $t(\mathbf{z})$ and $\mathbf{p}$,

$$p(\mathbf{p} \mid \mathbf{z}, \mathbf{v}) \cong \mathcal{N}\left(\mathbf{p}; t(\mathbf{z}) - G(\mathbf{v} - E[\mathbf{v}]), \frac{\partial t}{\partial \mathbf{z}}\mathbf{R}\frac{\partial t'}{\partial \mathbf{z}}\right), \tag{8}$$

where conditioning on $\mathbf{z}$ is the same as conditioning on $t(\mathbf{z})$. If we now substitute $\mathbf{x} = K\mathbf{p} + \overline{K}\mathbf{v}$,

$$\begin{aligned} E[\mathbf{x} \mid \mathbf{z}, \mathbf{v}] &= Kt(\mathbf{z}) - KG(\mathbf{v} - E[\mathbf{v}]) + \overline{K}\mathbf{v} \\ &= Kt(\mathbf{z}) + KGE[\mathbf{v}] + (\overline{K} - KG)\mathbf{v}, \\ \mathrm{Cov}[\mathbf{x} \mid \mathbf{z}, \mathbf{v}] &= K\frac{\partial t}{\partial \mathbf{z}}\mathbf{R}\frac{\partial t'}{\partial \mathbf{z}}K', \end{aligned} \tag{9}$$

we can approximate $\mathbf{x}$ as Gaussian with the above parameters as

$$p(\mathbf{x} \mid \mathbf{z}, \mathbf{v}) \cong \mathcal{N}\left(\mathbf{x}; Kt(\mathbf{z}) + KGE[\mathbf{v}] + (\overline{K} - KG)\mathbf{v},\ K\frac{\partial t}{\partial \mathbf{z}}\mathbf{R}\frac{\partial t'}{\partial \mathbf{z}}K'\right). \tag{10}$$

To get rid of the conditioning on $\mathbf{v}$, we appeal to Bayes' total probability theorem for continuous random variables, averaging over $\mathbf{v}$, we get

$$p(\mathbf{x} \mid \mathbf{z}) = \int p(\mathbf{x} \mid \mathbf{z}, \mathbf{v})\, p(\mathbf{v}) d\mathbf{v}. \tag{11}$$

Changing the conditioning and integrating the final pdf are given in

$$p(\mathbf{x} \mid \mathbf{z}) \cong \mathcal{N}\left(\mathbf{x}; Kt(\mathbf{z}) + \overline{K}E[\mathbf{v}],\ K\frac{\partial t}{\partial \mathbf{z}}\mathbf{R}\frac{\partial t'}{\partial \mathbf{z}}K' + (\overline{K} - KG)P(\overline{K} - KG)'\right), \tag{12}$$

with the approximate maximum a posteriori (MAP) estimator

$$\hat{\mathbf{x}} \cong E[\mathbf{x} \mid \mathbf{z}] = Kt(\mathbf{z}) + \overline{K}E[\mathbf{v}] \tag{13}$$

with covariance

$$\mathbf{P} \cong \mathrm{Cov}[\mathbf{x} \mid \mathbf{z}] = K\frac{\partial t}{\partial \mathbf{z}}\mathbf{R}\frac{\partial t'}{\partial \mathbf{z}}K' + (\overline{K} - KG)P(\overline{K} - KG)'. \tag{14}$$

2.5. MAP estimate using the unscented transform

To calculate $p(\mathbf{x} \mid \mathbf{z})$ in (12) we can replace the use of linearization typical for the extended Kalman filter, by using the unscented transform (UT) [9]. To calculate $p(\mathbf{x} \mid \mathbf{z})$ in the previous case, we used the first-order linearization of the functional relationships between $\mathbf{z}$, $\mathbf{v}$, and $\mathbf{p}$ which we had in $t(\mathbf{z})$ and $t \circ h(\mathbf{x})$.

Instead, we can directly derive a functional relationship of the measurements $\mathbf{z}$, the velocity vector $\mathbf{v}$, which is initialized by modeling assumptions, and the position $\mathbf{p}$. Using $\mathbf{z} = h(\mathbf{p}, \mathbf{v}) + \mathbf{w}$, we will solve for $\mathbf{p}$, that is, $\mathbf{p} = g(\mathbf{z} - \mathbf{w}, \mathbf{v})$, where the function g is in direct relationship to $t(\mathbf{z})$, since

$$g(\mathbf{z}, E[\mathbf{v}]) = t(\mathbf{z}). \tag{15}$$

Once we have this, usually nonlinear, functional relationship, we can use the unscented transform to derive $p(\mathbf{p} \mid \mathbf{z})$ from $p(\mathbf{z} - \mathbf{w}, \mathbf{v} \mid \mathbf{z})$, using the functional relationship in (15)

to map the influence of the measurement noise and the parameters modeled as random on the estimate of the other parameters.

To find the probability density of $p(\mathbf{z}-\mathbf{w},\mathbf{v}\mid\mathbf{z})$ we can use that $p(\mathbf{z}-\mathbf{w}\mid\mathbf{z})$ has mean $\mathbf{z}$ and covariance $\mathbf{R}$ and $p(\mathbf{v}\mid\mathbf{z},\mathbf{z}-\mathbf{w})$ is by modeling assumption $\mathcal{N}(\mathbf{v};0,P)$, since these parameters are assumed to be independent of the measurements. Due to conditional independence we get

$$p(\mathbf{z}-\mathbf{w},\mathbf{v}\mid\mathbf{z}) = p(\mathbf{z}-\mathbf{w}\mid\mathbf{z})\,p(\mathbf{v}\mid\mathbf{z},\mathbf{z}-\mathbf{w}) \tag{16}$$

which we can transform into $p(\mathbf{x}\mid\mathbf{z})$, using

$$\mathbf{x} = Kg(\mathbf{z}-\mathbf{w},\mathbf{v}) + \overline{K}\mathbf{v}. \tag{17}$$

To approximate a probability density at the output of a nonlinear transformation, $\boldsymbol{\zeta} = f(\boldsymbol{\chi})$, given the probability density at the input, for example, $\mathcal{N}(\boldsymbol{\chi};\mu_\chi,P_\chi)$, we apply the UT in the following way: we choose a set of $2n_\chi+1$ sigma points according to

$$\boldsymbol{\chi}^{(i)} = \mu_\chi \pm \sqrt{\frac{n_\chi}{1-W^{(0)}}}\left(\sqrt{P_\chi}\right)_j, \qquad \boldsymbol{\chi}^{(0)} = \mu_\chi, \tag{18}$$

where $j=1,\ldots,n_\chi$, $i=1,\ldots,2n_\chi$, and n_χ is the dimension of $\boldsymbol{\chi}$ [9]. (As pointed out by one of our reviewers, our notation in (18) is not very rigorous. In an abuse of notation we interpret $(\sqrt{P_\chi})_j$ as the jth eigen-vector scaled by the square root of the jth eigenvalue. When P_χ is diagonal our notation is freely adopted from Matlab.) Then we map each point via the nonlinear transform $\boldsymbol{\zeta}^{(i)} = f(\boldsymbol{\chi}^{(i)})$. The new set of points is used to approximate the mean and covariance of the probabilty density at the output of the nonlinear transform

$$\begin{aligned}\mu_\zeta &= \sum_{i=0}^{2n_\chi} W^{(i)}\boldsymbol{\zeta}^{(i)},\\ P_\zeta &= \sum_{i=0}^{2n_\chi} W^{(i)}\left(\boldsymbol{\zeta}^{(i)}-\mu_\zeta\right)\left(\boldsymbol{\zeta}^{(i)}-\mu_\zeta\right)',\end{aligned} \tag{19}$$

using a set of weights $W^{(0)} = 1/n_\chi$ and $W^{(i)} = (1-W^{(0)})/2n_\chi$ for $i=1,\ldots,2n_\chi$. Therefore, the relationship in (17) and the input probability density in (16) are everything we need to apply the UT.

3. TRACK INITIALIZATION FROM BEARINGS-ONLY MEASUREMENTS

3.1. Scenario description

In this scenario, only the spherical coordinates azimuth and elevation are measured; see Figure 1. Examples for this kind of scenario could be radar or sonar passive tracking of an emitting target, for example, a target using counter measures or active radar, sonar. Motivation to initialize from a small number of measurements could be a high-duty cycle of sensors, where it could take quite long to accumulate more measurements or a possibly urgent scenario where the target has to be tracked immediately, for example, an incoming projectile.

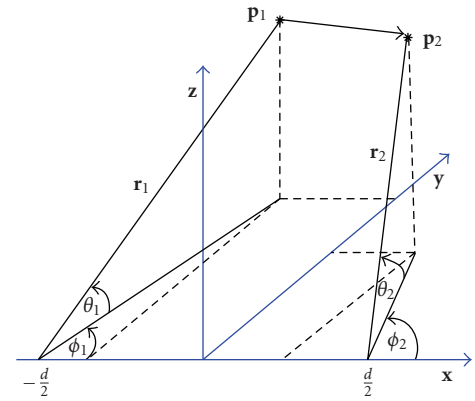

Figure 1: Bearings-only measurements scenario.

The formulation is generally enough to accommodate both, a scenario with several fixed sensors, possibly having a high-duty cycle of maybe 10–30 seconds, but only a small asynchronicity of maybe a few seconds; as well as a moving observer possibly engaged in an evasive maneuver.

Initializing from k generally asynchronous measurements is possible, if the measurements are taken at different positions $\mathbf{x}_s(n)$ [2]. For brevity without explicit dependency on n, $\mathbf{x} = [x,y,z,\dot{x},\dot{y},\dot{z}]'$ and $\mathbf{z} = [\phi,\theta]'$, the measurement equations are the following:

$$\phi = \arctan\left(\frac{y-y_s}{x-x_s}\right), \tag{20}$$

$$\theta = \arctan\left(\frac{z-z_s}{\sqrt{(x-x_s)^2+(y-y_s)^2}}\right). \tag{21}$$

To initialize the position only, $\mathbf{p} = [x,y,z]'$, it is sufficient to have only two measurements $k=2$, which gives us

$$k\eta_{\mathbf{z}} = 4 \geq \eta_{\mathbf{p}} = 3. \tag{22}$$

Those measurements should be taken from two distinct arbitrary points with distance d

$$\left|K'\left[\mathbf{x}_{s,1}-\mathbf{x}_{s,2}\right]\right| = d, \tag{23}$$

where $\mathbf{x}_{s,i}$, $i=1,2$ are the state vectors of the observer platform(s). Without loss of generality, we can assume the positions to be on the x-axis at $-d/2$ and $d/2$. Using

$$h(\mathbf{x}(n+1)-\mathbf{x}_s(n+1)) = h(F(n)\mathbf{x}(n)-\mathbf{x}_s(n+1)) \tag{24}$$

and defining $T = t_{n+1}-t_n$ as the time difference between the measurements, the equations can be expressed as

$$\begin{aligned}\phi_1 &= \arctan\left(\frac{y}{x+d/2}\right),\\ \theta_1 &= \arctan\left(\frac{z}{\sqrt{(x+d/2)^2+(y)^2}}\right),\\ \phi_2 &= \arctan\left(\frac{y+\dot{y}T}{x+\dot{x}T-d/2}\right),\\ \theta_2 &= \arctan\left(\frac{z+\dot{z}T}{\sqrt{(x+\dot{x}T-d/2)^2+(y+\dot{y}T)^2}}\right),\end{aligned} \tag{25}$$

depending only on $\mathbf{x}(n)$ and assuming constant velocity. In the following we will refer to $\mathbf{z}-\mathbf{w}=[\phi_1,\theta_1,\phi_2,\theta_2]'$ as the stacked vector of the true measurements to simplify notation.

3.2. Analytical solution for different measurement subsets

We avoid an underdetermined equation system by making statistical assumptions about the velocity, $\mathbf{v}=[\dot{x},\dot{y},\dot{z}]'$. The velocity will be assumed to be zero-mean Gaussian distributed $\mathcal{N}(\mathbf{v};0,P)$, which is reasonable since there is no preferred direction; the elements of P are usually chosen between half and the full maximum speed of possible targets.

Since we have $k\eta_{\mathbf{z}}=4>\eta_{\mathbf{p}}=3$, we have to drop one measurement to avoid an overdetermined equation system ($n=1$). Accordingly, we can choose both azimuth measurements with either elevation or both elevation with either azimuth, leading to four different inverse functions.

Now if we solve (2) for $\mathbf{p}$, we get

$$\mathbf{p}=t(\mathbf{z}-\mathbf{w})+f(\mathbf{v},\mathbf{z}-\mathbf{w}), \tag{26}$$

where we choose f such that $f(E[\mathbf{v}],\mathbf{z}-\mathbf{w})=0$. This approach will be consequently applied to all four possible combinations of three measurements.

3.2.1. Two azimuths and one elevation

Using $\{\phi_1,\phi_2,\theta_1\}$ of (25) and solving for $\mathbf{p}$ we first solve for

$$\begin{aligned}x&=\frac{\dot{x}T\tan\phi_2-\dot{y}T-d/2(\tan\phi_1+\tan\phi_2)}{\tan\phi_1-\tan\phi_2}\\&=d\frac{\sin\phi_1\cos\phi_2}{\sin(\phi_2-\phi_1)}+\frac{d}{2}-T\cos\phi_1\frac{\dot{x}\sin\phi_2-\dot{y}\cos\phi_2}{\sin(\phi_2-\phi_1)},\\y&=\frac{(\dot{x}T-d)\tan\phi_1\tan\phi_2-(\dot{y}T)\tan\phi_1}{\tan\phi_1-\tan\phi_2}\\&=d\frac{\sin\phi_1\sin\phi_2}{\sin(\phi_2-\phi_1)}-T\sin\phi_1\frac{\dot{x}\sin\phi_2-\dot{y}\cos\phi_2}{\sin(\phi_2-\phi_1)}.\end{aligned} \tag{27}$$

From which we now calculate z as

$$\begin{aligned}z&=\tan(\theta_1)\sqrt{(x+d/2)^2+y^2}\\&=\tan(\theta_1)\left|\frac{d\sin\phi_2}{\sin(\phi_2-\phi_1)}-T\frac{\dot{x}\sin\phi_2-\dot{y}\cos\phi_2}{\sin(\phi_2-\phi_1)}\right|.\end{aligned} \tag{28}$$

The first inverse function $t_1(\mathbf{z}-\mathbf{w})$ is accordingly

$$t_1(\mathbf{z}-\mathbf{w})=\begin{pmatrix}d\dfrac{\sin\phi_1\cos\phi_2}{\sin(\phi_2-\phi_1)}+\dfrac{d}{2}\\[2ex]d\dfrac{\sin\phi_1\sin\phi_2}{\sin(\phi_2-\phi_1)}\\[2ex]\tan(\theta_1)\left|\dfrac{d\sin\phi_2}{\sin(\phi_2-\phi_1)}\right|\end{pmatrix} \tag{29}$$

where we used ϕ_1, θ_1, and ϕ_2 to estimate $\mathbf{p}$; then $\mathbf{x}$ is $Kt_1(\mathbf{z}-\mathbf{w})+\overline{K}E[\mathbf{v}]$.

To calculate the covariance matrix according to (14) we need the partial derivatives $\partial t_1/(\partial\mathbf{z}-\mathbf{w})$ and $\partial t_1\circ h/\partial\mathbf{p}$, which can be found in Appendix A.

Alternatively, we can use the unscented transform (UT) for which we need to find a function g which maps from $\mathbf{v}$ and $\mathbf{z}-\mathbf{w}$ to $\mathbf{p}$. This function g_1 is already available in (27), (28), that is, $\mathbf{p}=g_1(\mathbf{z}-\mathbf{w},\mathbf{v})$. So we are able to directly apply the UT as described in Section 2.5.

The estimation function t_2 for $\{\phi_1,\phi_2,\theta_2\}$ can be calculated by changing $\phi_1\leftrightarrow\phi_2$, $\theta_1\leftrightarrow\theta_2$, and $d\leftrightarrow -d$ due to the symmetry of the scenario. For the covariance we also substitute $T\leftrightarrow -T$.

3.2.2. One azimuth and two elevations

As the other possibility to calculate $\mathbf{p}(n)$, we can use $\{\phi_1,\theta_1,\theta_2\}$ of (25). Substituting (see Figure 1)

$$\begin{aligned}x&=\rho_1\cos\phi_1-\frac{d}{2},\\y&=\rho_1\sin\phi_1,\\z&=\rho_1\tan\theta_1\end{aligned} \tag{30}$$

with the ground range from sensor one ρ_1, starting from the definition of θ_2, we get

$$\tan^2\theta_2=\frac{(\rho_1\tan\theta_1+\dot{z}T)^2}{(\rho_1\cos\phi_1-d+\dot{x}T)^2+(\rho_1\sin\phi_1+\dot{y}T)^2}. \tag{31}$$

This is a quadratic equation in ρ_1; using $q=\tan\theta_2/\tan\theta_1$ for simpler notation we reformulate as

$$\begin{aligned}&\rho_1^2(1-q^2)\\&\quad+2\rho_1(\cot\theta_1\dot{z}T+q^2(\cos\phi_1(d-\dot{x}T)-\sin\phi_1\dot{y}T))\\&\quad+\cot^2\theta_1\dot{z}^2T^2-q^2((d-\dot{x}T)^2+\dot{y}^2T^2)=0.\end{aligned} \tag{32}$$

Setting $T=0$ (equivalent to replacing $\mathbf{v}$ with $E[\mathbf{v}]=\mathbf{0}$) we can calculate the inverse function by solving first for ρ_1,

$$\rho_1^2(1-q^2)+2d\rho_1q^2\cos\phi_1-q^2d^2=0. \tag{33}$$

For $q=1$ we get

$$\rho_1=\frac{d}{2\cos\phi_1} \tag{34}$$

and else

$$\rho_1=d\left(-\frac{q^2\cos\phi_1}{1-q^2}\pm\left|\frac{q}{1-q^2}\right|\sqrt{1-q^2\sin^2\phi_1}\right). \tag{35}$$

To solve this ambiguity we use the second azimuth ϕ_2. For geometrical reasons, if $q^2<1$, there is only one solution (which is positive). Otherwise, $q^2>1$, we choose the positive root if $|\phi_2|<\pi/2$ and the negative else. The interested reader can read our detailed argument in Appendix A.

The derivatives needed to calculate the covariance can be found in Appendix A.

To calculate the covariance matrix for t_3 using the unscented transform (UT), we have to solve (32) for ρ_1, without setting $T = 0$. This still means solving a quadratic equation, but is notational more cumbersome. Inserting the solution into (30) yields g_2.

The last estimation functions t_4 for $\{\phi_2, \theta_1, \theta_2\}$ can be calculated through the function $t_3(\mathbf{z}-\mathbf{w})$ by changing $\phi_1 \leftrightarrow \phi_2$, $\theta_1 \leftrightarrow \theta_2$, and $d \leftrightarrow -d$. And for the covariance we also substitute $T \leftrightarrow -T$.

4. TRACK INITIALIZATION FROM RANGE AND AZIMUTH

4.1. Scenario description

Traditional active radars give range measurements and sometimes only partial bearings. This is usually not a problem if the setup can be approximated by a 2-dimensional interpretation. Even so, the increased uncertainty should be incorporated in the covariance, which is a good reasoning to apply our approach.

Again we will use $k = 2$ measurements to estimate the position and make statistical assumptions about the velocity. The measurement model for range and azimuth is as follows:

$$r = \sqrt{(x - x_s)^2 + (y - y_s)^2 + (z - z_s)^2} \tag{36}$$

and ϕ is defined as in (20). As in Section 3, the measurements are taken d apart with time difference T. Since we have $k\eta_{\mathbf{z}} > \eta_{\mathbf{p}}$, we will be able to choose four different functions t_i, either two azimuth angles and one range measurement or two range measurements and one azimuth angle.

4.2. Analytical solution for different measurement subsets

4.2.1. Two azimuths and one range

Using $\{r_1, \phi_1, \phi_2\}$ we get the same results for x, y as in the previous section, see (27). Solving for z, we get

$$\begin{aligned} z &= \sqrt{r_1^2 - (x + d/2)^2 - y^2} \\ &= \sqrt{r_1^2 - \left(d\frac{\sin\phi_2}{\sin(\phi_2 - \phi_1)} - T\frac{\dot{x}\sin\phi_2 - \dot{y}\cos\phi_2}{\sin(\phi_2 - \phi_1)}\right)^2} \end{aligned} \tag{37}$$

and accordingly $t_1(\mathbf{z} - \mathbf{w})$ varies from (29) only in the last component.

The linearizations necessary to compute the covariance can be found in Appendix B.

To use the unscented transform (UT) we need g. In this case, the function is readily available in (27) and (37), which leads to immediate applicability.

The function t_2 can be generated from t_1, by replacing $r_1 \leftrightarrow r_2$, $\phi_1 \leftrightarrow \phi_2$, and $d \leftrightarrow -d$ as the setup is symmetric again. To calculate the covariance also $T \leftrightarrow -T$ has to be exchanged.

4.2.2. One azimuth and two ranges

To calculate $t_2(\mathbf{z} - \mathbf{w})$, we use $\{r_1, r_2, \phi_1\}$. First we use r_1, r_2 which is geometrically speaking the intersection of two spheres. Solving for x and taking the expectation over $\dot{x}$, $\dot{y}$, $\dot{z}$, we get

$$x = \frac{r_1^2 - r_2^2 + (2\sigma_v^2 + \sigma_h^2)T^2}{2d}. \tag{38}$$

The solution for x is unambiguous since the intersection is a circle normal to and centered on the line connecting the centers of the spheres, which coincides with the x-axis. To solve for y, we use the definition of ϕ,

$$\begin{aligned} y &= (x + d/2)\tan\phi_1 \\ &= \frac{r_1^2 - r_2^2 + (2\sigma_v^2 + \sigma_h^2)T^2 + d^2}{2d}\tan\phi_1 \end{aligned} \tag{39}$$

and similarly the definition of r to solve for z,

$$\begin{aligned} z &= \sqrt{r_1^2 - (x + d/2)^2 - y^2} \\ &= \sqrt{r_1^2 - \left(\frac{r_1^2 - r_2^2 + (2\sigma_v^2 + \sigma_h^2)T^2 + d^2}{2d}\right)^2 (1 + \tan^2\phi_1)}, \end{aligned} \tag{40}$$

where we disregard the ambiguity towards $\pm z$, since we can assume positive z. Finally, the complete function is

$$t_3(\mathbf{z} - \mathbf{w}) = \begin{pmatrix} \rho_1\cos\phi_1 - d/2 \\ \rho_1\sin\phi_1 \\ \sqrt{r_1^2 - \rho_1^2} \end{pmatrix} \tag{41}$$

with

$$\rho_1 = \frac{r_1^2 - r_2^2 + (2\sigma_v^2 + \sigma_h^2)T^2 + d^2}{2d\cos\phi_1}. \tag{42}$$

We can see that if the z component turns complex, there is no solution. This usually happens if the radii do not render an intersection of the two spheres or the azimuth is off too far, due to measurement errors or the unknown speeds.

The linearizations to calculate the covariance can be found in Appendix B.

Calculating the covariance matrix with unscented transform in this case is quite complicated. Setting $\dot{z} = 0$ simplifies this somewhat (this can be justified if the velocity in elevation is assumed to be smaller than velocity in plane),

$$\begin{aligned} \left(x + \frac{d}{2}\right)^2 + y^2 + z^2 &= r_1^2, \\ \left(x + \dot{x}T - \frac{d}{2}\right)^2 + (y + \dot{y}T)^2 + z^2 &= r_2^2, \\ \tan\phi_1 &= \frac{y}{x + d/2}, \\ \left(x + \frac{d}{2}\right)^2 - \left(x + \dot{x}T - \frac{d}{2}\right)^2 + y^2 - (y + \dot{y}T)^2 &= r_1^2 - r_2^2. \end{aligned} \tag{43}$$

Setting

$$Q = \left(\frac{d}{2}\right)^2 - \left(\dot{x}T - \frac{d}{2}\right)^2 - (\dot{y}T)^2 - r_1^2 + r_2^2, \tag{44}$$

we get

$$x\left(d - \left(2\left(\dot{x}T - \frac{d}{2}\right)\right)\right) - 2y\dot{y}T + Q = 0, \tag{45}$$

with $y = \tan(\phi_1)(x + d/2)$ we can calculate

$$x = \frac{\tan(\phi_1)d\dot{y}T - Q}{(d - 2(\dot{x}T - d/2)) - 2\tan(\phi_1)\dot{y}T} \tag{46}$$

which leads to y and z. The application onto g_3 is straightforward afterwards.

The function t_4 can be generated from t_3 again, by replacing $r_1 \leftrightarrow r_2$, $\phi_1 \leftrightarrow \phi_2$, and $d \leftrightarrow -d$ due to the symmetric setup. To calculate the covariance also $T \leftrightarrow -T$ has to be exchanged.

5. NUMERICAL RESULTS

5.1. Simulation setup

This section will give a detailed comparison of the methods derived previously. We will give Monte Carlo simulation results varying over different parameters and evaluate the performance based on the average estimation error. Maybe more importantly, we will check the consistency of the estimates with the derived covariance matrices and see how well they can be used to determine the optimal initial measurement subset.

5.1.1. Average estimation error

The root-mean-square error of the position estimate (RMSPOS) is an absolute error measure and direct performance criteria. It is averaged over all simulation runs. The RMS error from N monte Carlo runs for a position error $\tilde{\mathbf{p}} = \hat{\mathbf{p}} - \mathbf{p}$ is

$$\mathrm{RMS}(\mathbf{p}) = \sqrt{\frac{1}{N}\sum_{i=1}^{N} |\tilde{\mathbf{p}}_i|^2}. \tag{47}$$

5.1.2. Crámer-Rao lower bound

Since we consider nonlinear measurements and additive white Gaussian noise, the Crámer-Rao lower bound (CRLB) can be derived in a standard way. The general calculation of the Fisher information matrix $\mathbf{J}_0$ as in [3] can be replaced by the more specialized formula

$$\begin{aligned}\mathbf{J}_0 &= E\left\{\left[\frac{\partial}{\partial \mathbf{x}}\log\Lambda(\mathbf{x})\right]\left[\frac{\partial}{\partial \mathbf{x}}\log\Lambda(\mathbf{x})\right]'\right\} \\ &= \frac{\partial h}{\partial \mathbf{x}}[\mathrm{Cov}(\mathbf{w})]^{-1}\frac{\partial h'}{\partial \mathbf{x}},\end{aligned} \tag{48}$$

where $\Lambda(\mathbf{x}) = p(\mathbf{z} \mid \mathbf{x})$ is the likelihood function. Unfortunately, for a minimum number of measurements, the matrix $\mathbf{J}_0$ will usually not be invertible. This reflects that we cannot estimate the full-state vector $\mathbf{x}$ without additional assumptions. As information is additive, these additional assumptions, usually in the form of a prior distribution on $\mathbf{v}$, can be added to the Fisher information matrix [10],

$$\mathbf{J} = \mathbf{J}_0 + \mathbf{J}_P, \tag{49}$$

where $\mathbf{J}_P$ is the Fisher information of the prior. Assuming a Gaussian prior on $\mathbf{v}$, this will take the following form:

$$\mathbf{J}_P = \begin{bmatrix} 0 & 0 \\ 0 & P^{-1} \end{bmatrix}. \tag{50}$$

5.1.3. Consistency

Filter consistency is usually measured using the normalized (state) estimation error squared (NEES), defined as

$$\epsilon = \tilde{\mathbf{x}}'\mathbf{P}^{-1}\tilde{\mathbf{x}} \tag{51}$$

which should be chi-square distributed with $\eta_{\mathbf{x}}$ degrees of freedom if the filter is consistent. In Monte Carlo simulations that provide N independent samples ϵ_i, $i = 1, \ldots, N$, the average NEES is

$$\bar{\epsilon} = \frac{1}{N}\sum_{i=1}^{N}\epsilon_i, \tag{52}$$

where now the test is on if $N\bar{\epsilon}$ is chi-square distributed with $N\eta_{\mathbf{x}}$ degrees of freedom. This hypothesis is accepted if $N\bar{\epsilon}$ is in the appropriate acceptance region. In all examples, we will use a 95% acceptance region.

5.1.4. Decision regions

Since our approach uses only a subset of the available measurements, merging the leftover measurements using Kalman filter steps, we need to pick the best subset to start out with. The optimality criterion we use is the trace of the covariance matrix. For geometric reasons, usually the same subset is picked over a larger region; we will be interested to see these.

5.1.5. Maximum a posteriori solution

As a baseline comparison we include a numerical maximum a posteriori (MAP) solution. It is found by maximizing the following density:

$$p(\mathbf{z}, \mathbf{x}) = p(\mathbf{z} \mid \mathbf{x})p(\mathbf{x}), \tag{53}$$

where $p(\mathbf{z} \mid \mathbf{x}) = \mathcal{N}(\mathbf{z}; h(\mathbf{x}), \mathbf{R})$ and $p(\mathbf{x}) = p(\mathbf{p}, \mathbf{v})$ are Gaussian with covariance P in $\mathbf{v}$, but uniform over the observation region V in $\mathbf{p}$,

$$p(\mathbf{p}, \mathbf{v}) = \frac{1}{|V|}\cdot\frac{1}{|2\pi P|^{1/2}}\exp\left(-\frac{1}{2}\mathbf{v}'P^{-1}\mathbf{v}\right). \tag{54}$$

Since the uniform density only concerns the search space, the problem reduces to a nonlinear least-squares problem by minimizing the negative logarithm instead:

$$\min_{\mathbf{x}}[\mathbf{z} - h(\mathbf{x})]'\mathbf{R}^{-1}[\mathbf{z} - h(\mathbf{x})] + [\overline{K}'\mathbf{x}]'P^{-1}[\overline{K}'\mathbf{x}]. \tag{55}$$

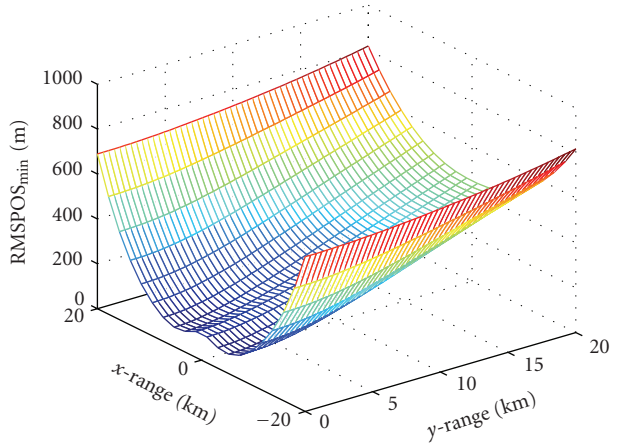

Figure 2: Cramér-Rao lower bound (CRLB) for a target altitude of $z = 4$ km and asynchronous measurements $T = 2$ seconds.

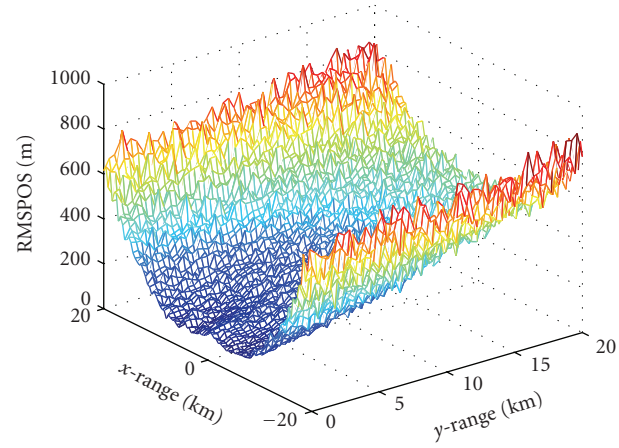

Figure 3: Result of the numerical maximum a posterori (MAP) estimator for a target altitude of $z = 4$ km and asynchronous measurements $T = 2$ seconds.

5.2. Bearings-only measurements

As described in Section 3, the sensors are located at $\pm d/2$, where we choose $d = 10$ km for our numerical example. We plot results for a symmetric x/y half-plane of 40 km by 20 km and pick a constant target altitude for each simulation. The two sets of measurements needed in this scenario are taken with an arbitrary time difference T which is usually in the range of a few seconds and the target is assumed to move with constant speed within this time interval. The speeds are random with $\dot{x}$, $\dot{y}$, $\dot{z}$ assumed independent and $\dot{x}$, $\dot{y}$ with the same $\sigma_v = 100$ m/s and $\dot{z}$ with $\sigma_h = 10$ m/s. Other parameters are the measurement noises, σ_ϕ, σ_θ, which are both 2 mrad $\approx 0.1^\circ$ and the number of Monte Carlo runs $N = 10^3$.

To be able to evaluate our algorithms, we first take a look at the CRLB to understand the geometry of this setup. As an example, we plot the CRLB for position estimation accuracy in Figure 2 for an offset of $T = 2$ seconds between the two measurements and a target altitude of $z = 4$ km. We can see that the estimation accuracy is notably higher when the target is "between" the sensors, that is, along the $x = 0$ km axis. This effect is less noticeable for larger target altitudes, but increases if targets are at lower altitudes. To understand the geometry of this effect, we must realize that the angular information we have represented two rays originating from the sensor positions. If the two rays are close to parallel, the estimation accuracy will be low—contrary the estimation accuracy will be high if the rays are close to perpendicular.

As a baseline comparison, we also plot the results using a numerical MAP estimator. Solving (55) via a standard gradient-based nonlinear least-squares solver, we get the following results (see Figure 3). We see that the MAP estimates meet the performance predicted by the CRLB. Our following algorithms will aim to achieve the same performance at a lower computational complexity. At the end of this section we will explicitly compare average run times and complexity.

We run both implementations of our initialization algorithm. The RMSPOS can be seen in Figure 4(a) using the extended Kalman filter (EKF) linearization and Figure 4(c) for the unscented transform (UT). Comparing to the CRLB in Figure 2, the differences are minor. Both implementations achieve a performance practically meeting the bound. An interesting artifact both implementations share is a ridge arcing from the sensor positions outwards to both sides—we will come back to this later. The only difference is that the UT has some barely noticeable artifacts in the RMSPOS when the target is in the area right above the sensors.

Next we inspect the consistency of the estimation error with the calculated covariance. The consistency is evaluated using the normalized estimation error squared (NEES), which is calculated using the full estimation error vector. Even though $\mathbf{v}$ is not actually estimated, we include it in the NEES calculation to check the consistency of the cross correlation. The NEES for both implementations is plotted in Figures 4(b)–4(d), since the state vector $\mathbf{x}$ has six components, the 95% acceptance region is around six—both figures are largely consistent. Above the sensor positions the estimates are inconsistent, which is connected to some of the derivatives of the measurement equations approaching infinity for zero ground range. Comparing the EKF/UT implementations, the nonconsistent region around the sensor position is somewhat larger for the EKF.

To give an example of which subset of measurements has the best initialization geometry, we plot the choices in Figure 5 for the EKF implementation (there is no visible difference to the UT). The values $i = 1, 2, 3, 4$ depict which initialization function t_i is used in which region. Intuitively, the regions are symmetric as we chose the functions t_i. The functions using two azimuth angles (t_1, t_2) dominate most of the area, while the functions using two elevation angles (t_3, t_4) are mainly used when the target is close to the $y = 0$ km line. This seems sensible and coincides with our understanding of the sensor/target geometry, as both sensors are located on this line and intersecting two azimuth rays becomes more and more error sensitive as they become close to parallel.

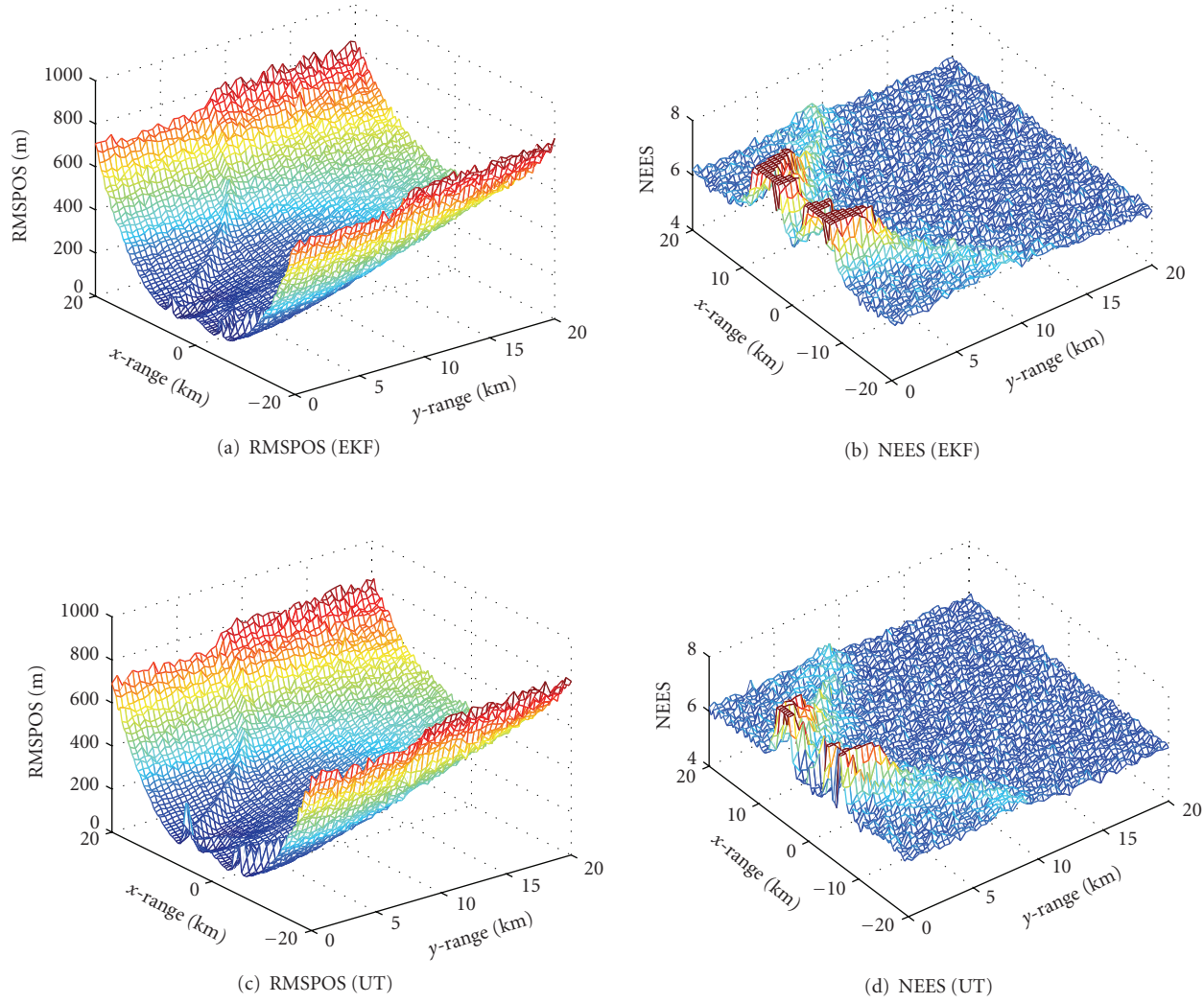

(a) RMSPOS (EKF)

(b) NEES (EKF)

(c) RMSPOS (UT)

(d) NEES (UT)

FIGURE 4: Comparing extended Kalman filter (EKF) and unscented transform (UT) implementation for $z = 4\,\text{km}$ and $T = 2$ seconds the differences are minor; the RMSPOS of the UT has a small additional artifact, while the EKF NEES has slightly worse consistency around the sensor positions.

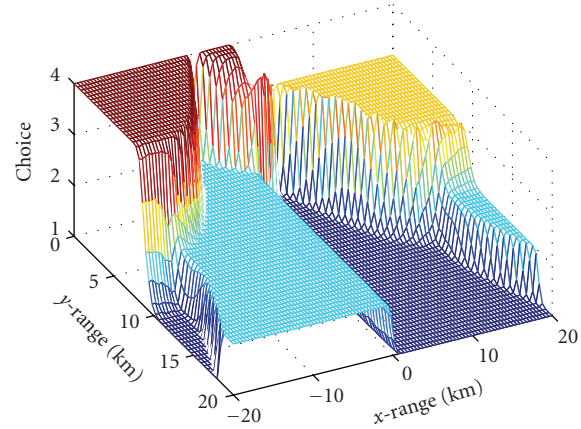

FIGURE 5: Decision regions for a target altitude of $z = 4\,\text{km}$ and asynchronous measurements $T = 2$ seconds. The values $i = 1, 2, 3, 4$ on the z-axis (labeled "choice") depict the four possible initialization functions t_i.

Comparing Figure 5 to Figures 4(a)–4(c), the aforementioned ridges in the RMSPOS coincide with decision boundaries. These ridges are not present in the CRLB, apparently the perturbation due to unknown velocity and/or measurement noise can lead to choosing a suboptimal subset, increasing the estimation error.

For larger measurement errors $\sigma_\phi = \sigma_\theta = 20\,\text{mrad} \approx 1°$, the first part of (14) scales proportionally. Since the errors due to the unknown velocity are less position dependent than velocity dependent, the errors introduced through the velocity are almost constant in the plane (we average over randomly drawn velocities). The plot of the CRLB in Figure 7 and the plots in Figure 6 confirm that the estimation errors scale with the measurement errors without changing much the geometry. Inspecting the NEES we see categorically different behaviors between the two implementations. The EKF has closed regions where the NEES is far outside the 95% acceptance region (see Figure 6(b)). Thesecoincide with the re-

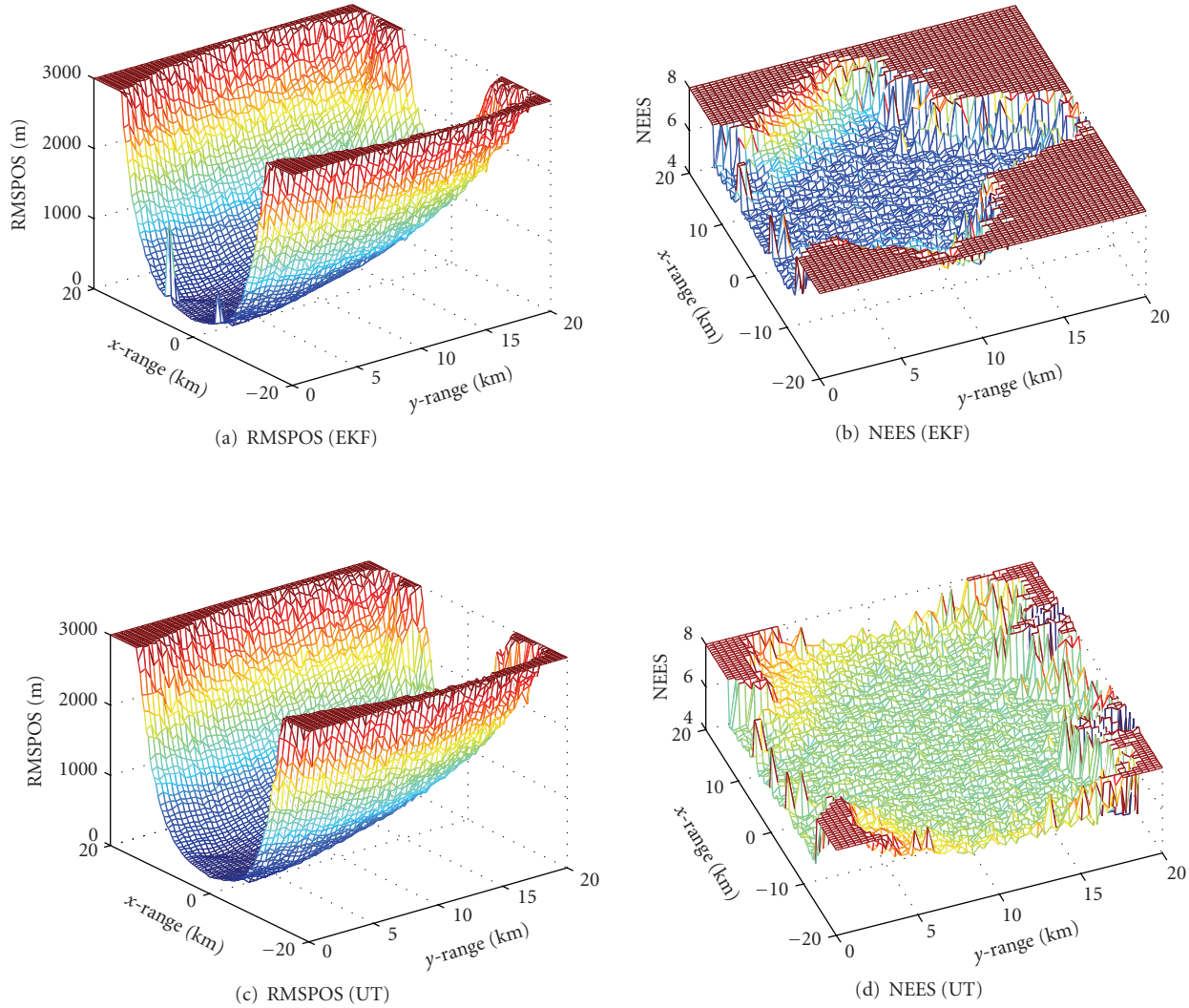

Figure 6: For larger measurement errors of ≈1°, the differences between EKF (a), (b) and UT (c), (d) become obvious, especially in consistency they have categorically different behavior ($z = 4$ km and $T = 2$ seconds).

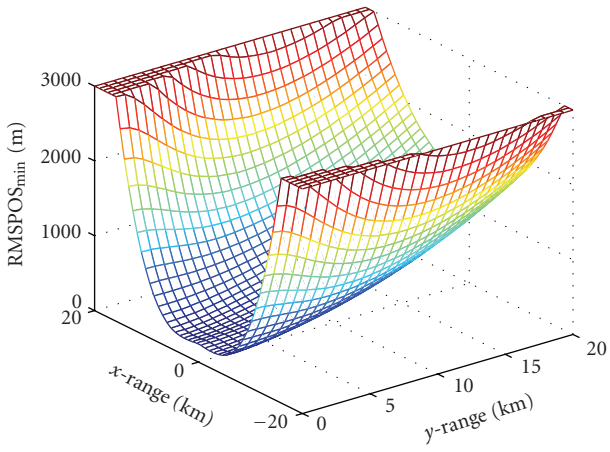

Figure 7: Cramér-Rao lower bound (CRLB) for a target altitude of $z = 4$ km and asynchronous measurements of $T = 2$ s with large measurement errors (≈1°).

gions when the RMSPOS is very high, compare Figure 6(a), from this we figure that for very large errors the linearizations used to determine the covariance are no longer accurate. The UT has better consistency, although also with some nonconsistent regions.

5.3. Range and azimuth measuements

The setup for position initialization from two measurements is basically the same as in Section 5.2. The sensors are on the x-axis with distance $d = 10$ km, we simulate over a halfplane, the assumed distribution of the velocity is the same, noise variance is $\sigma_\phi \approx 0.1^\circ$ and $\sigma_r = 65$ m.

We will look at a larger altitude of $z = 8$ km and time offset of $T = 2$ seconds. The CRLB is plotted in Figure 9 to inspect the sensor target geometry; for the chosen range standard deviation of $\sigma_r = 65$ m and same azimuth precision, the estimation error is generally higher compared to the

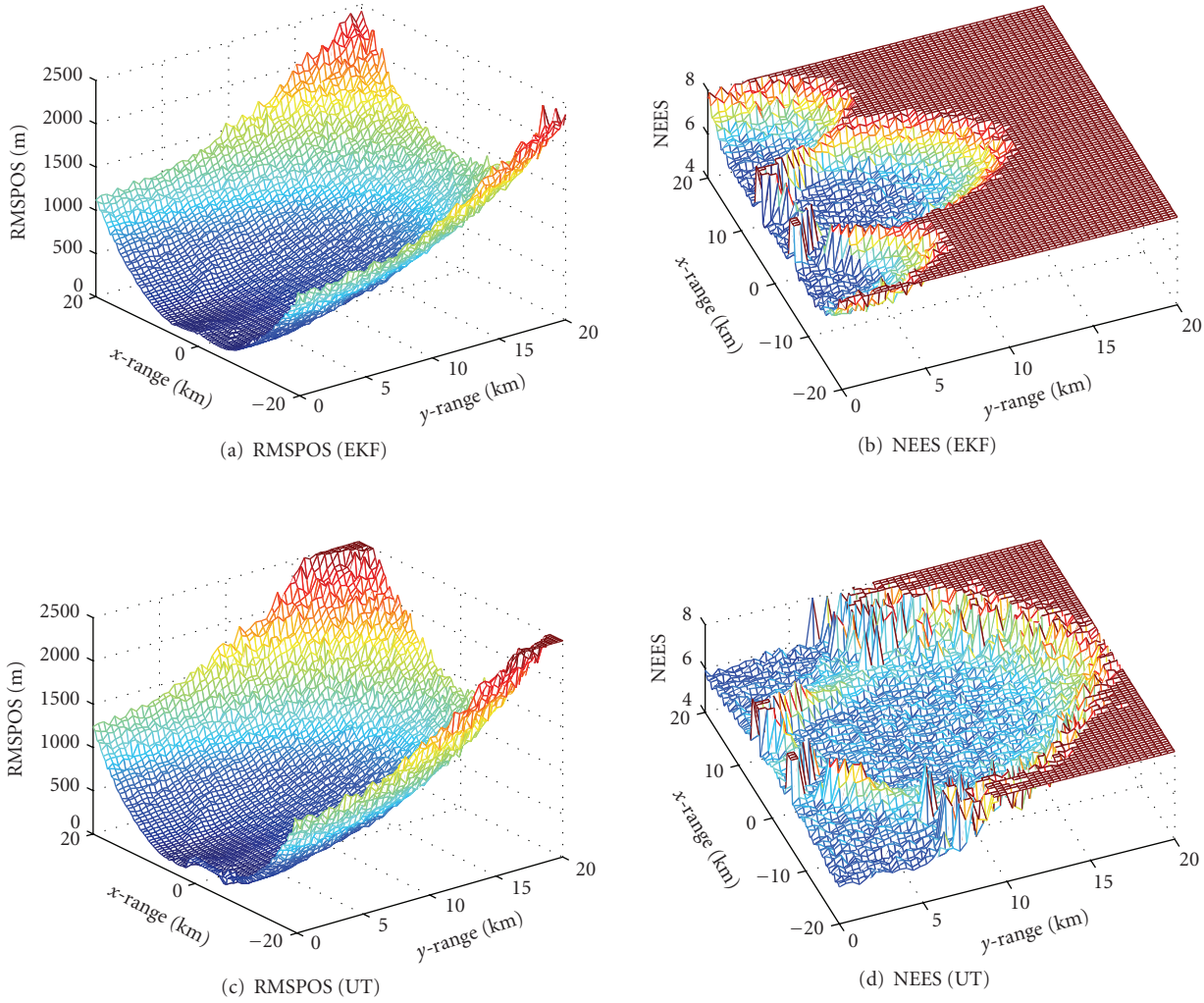

(a) RMSPOS (EKF)

(b) NEES (EKF)

(c) RMSPOS (UT)

(d) NEES (UT)

Figure 8: In the slant range and azimuth scenario the differences between EKF and UT are obvious. For a target altitude of $z = 8$ km and $T = 2$ seconds the EKF is not consistent due to the large errors, while still achieving good estimation performance.

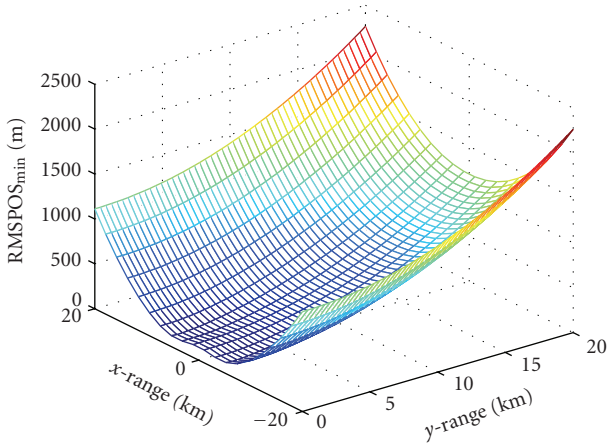

Figure 9: CRLB for a target altitude of $z = 8$ km and asynchronous ($T = 2$ seconds) measurements of range and azimuth.

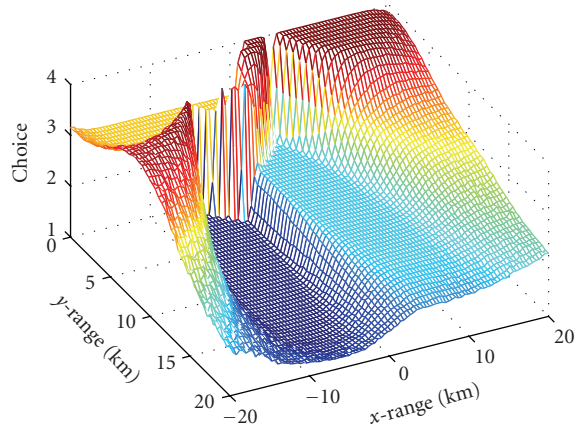

Figure 10: Decision regions for a target altitude of $z = 8$ km and asynchronicity of $T = 2$ seconds.

bearings-only scenario. Especially for positions far from the sensors the errors increase much stronger.

Again we compare the two implementations of our algorithm, namely, the EKF versus the UT. In Figures 8(a)–8(c) we can see that as dictated by the CRLB the position estimation error is noticeably higher compared to the bearings-only scenario. Both implementations reach the CRLB for the most part, except for regions with very large error. The only difference is that the UT has slightly larger errors towards the far corners of the plane. The consistency of the two implementations is very different, compare Figures 8(b)–8(d); in both cases there are regions of dramatically too small covariance (the figures are capped at eight), but the consistent regions of the UT are much larger.

The decision regions are plotted in Figure 10; foremost, the transition between different decision regions is more diffuse. This can be credited to the generally higher errors, leading more often to a choice of suboptimal initialization or to no solutions in some of the nonlinear equations.

5.4. Summary of differences between EKF and UT

The EKF linearization and UT are both ways to handle nonlinearities. In our scenarios, we implemented both approaches and compared their performance.

Except for minor artifacts, we observe noticeable differences only in case of large estimation errors (inherent to the measurement geometry as confirmed by the CRLB). These large estimation errors are caused either by large measurement errors as in Figure 6 or by difficult geometry, compare Figure 8. (Similarly large estimation errors could also be caused by strong aberration of the modeled parameter from its expectation, as in high velocity targets or large asynchronicity T. No plots of this were included, but we found inherently the same behavior.) In these cases, we notice enlarging regions were the estimates are not consistent with the calculated covariance and the estimation error does not always achieve the CRLB.

In direct comparison, the UT seems to have better consistency in these cases than the EKF linearization, that is, the regions in which the estimates are not consistent with the calculated covariance are always smaller. On the other hand, the estimation errors of the EKF-based implementation are closer to the CRLB, that is, less divergence from the CRLB for very large estimation errors in Figure 6 and especially in Figure 8.

We figure from these observations that the EKF has worse consistency, but the UT's estimation accuracy is directly affected by an inconsistent covariance. While the consistency problems of the EKF can be explained with the inaccuracy of the linearization for large deviations, the increasing artifacts and estimation errors of the UT are more difficult to analyze.

Since both approaches include solving nonlinear equations, which might not have a solution, sometimes it is not possible to generate an estimate and/or suited covariance matrix for one or several subsets of measurements. This is usually caused by the measurement errors and/or additional perturbation through "random" parameters. Therefore, we adapted both methods to work with cases where there is no solution, implemented in the estimation function t or transformation function g.

Table 1: Complexity comparison between EKF, UT, and gradient-based MAP.

	EKF	UT	MAP
Computation time	2.4 ms	9.6 ms	255 ms

In the easiest case, if a subset of measurements leads to no solution, we simply set the covariance matrix to infinity, effectively removing this subset from the following selection. This can lead to using measurements with a bad geometry, which would have ordinarily not been selected. In this case, usually the covariance matches well, while the estimation error does not meet the CRLB. To bypass this, we have tried to define solutions to nonlinear equations which can lead to an improved estimation error, but in turn leads to problems generating a covariance matrix.

The superior performance of the UT to determine a suited covariance is directly connected to evaluating points in a surrounding of the expected value, while linearization only evaluates curvature information at this point. This can be a drawback in the sense that the UT is confronted more often with the case of no solution to the nonlinear equations. For example, when intersecting two spheres in one case of Section 4 measurement errors can lead to too small radii which do not intersect. While the actual measurements might still lead to a solution, which is good enough for the EKF, evaluating points about one standard deviation away for the UT will more likely lead to no solution.

5.5. Complexity analysis

In the literature, the complexity of one Kalman filter iteration using the UT is deemed on the same order as an iteration using the EKF linearization [9]. In our particular case, we do not execute a full Kalman filter iteration and therefore do not need to invert a matrix. Accordingly, our EKF-based implementation has lower complexity than the UT implementation, compare Table 1. The EKF-based implementation only evaluates the mean and covariance for each of the possible measurement combinations. The UT evaluates functions of similar complexity for each of its points, compare (18). The EKF proves to be about four times as fast, where for both EKF and UT we used implementations in Matlab, most likely leaving room for performance improvement.

Next we compare the run-time to a nonlinear numerical MAP solution. Since exhaustive search is of prohibitive complexity, we applied a gradient-based nonlinear least-squares algorithm supplied by the Matlab optimization toolbox. The performance seems reasonable, as the algorithm involves many iterations consisting of evaluating both MAP function and its gradient. The numerical MAP algorithm is only one order of magnitude slower than the UT implementation, although not significant in absolute numbers, if many evaluations are necessary this complexity difference is definitely nonnegligible.

6. CONCLUSION

We have provided a general approach for initialization, applicable to a large range of estimation problems using small sets of noninvertible measurements. The approach allows modeling some parameters statistically to reduce the dimension of the estimation problem. This way we can initialize also in scenarios where observability would otherwise not be given. Additionally, to reduce complexity we initialize only from a subset of measurements to avoid an overdetermined equation system. This enormously reduced complexity as no optimization algorithm has to be used and we simply insert the measurements in several equations. To minimize the information loss of using less measurements we use an optimality criterion to choose the best subset of measurements to initialize from and incorporate leftover measurements afterwards using Kalman filter steps. A covariance matrix has been derived analytically to describe the estimation errors. The covariance accounts explicitly for uncertainties related to reducing the estimation problem and can be used to find the best subset of measurements for initialization.

We included a detailed discussion and numerical analysis of examples using Cramèr-Rao lower bounds and Monte Carlo simulation for performance comparison and proof of consistency. The examples included 3D initialization scenarios of incomplete spherical measurements, bearings-only or slant-range, and azimuth.

APPENDICES

A. BEARINGS-ONLY SCENARIO

A.1. Derivatives for two azimuth, one elevation

Differentiating (29) we get

$$\frac{\partial t_1}{\partial \mathbf{z}-\mathbf{w}} = \begin{pmatrix} d\dfrac{\sin\phi_2\cos\phi_2}{\sin^2(\phi_2-\phi_1)} & 0 & -d\dfrac{\sin\phi_1\cos\phi_1}{\sin^2(\phi_2-\phi_1)} & 0 \\ d\dfrac{\sin^2(\phi_2)}{\sin^2(\phi_2-\phi_1)} & 0 & -d\dfrac{\sin^2(\phi_1)}{\sin^2(\phi_2-\phi_1)} & 0 \\ \dfrac{\partial\rho_1}{\partial\phi_1}\tan\theta_1 & \rho_1/\cos^2\theta_1 & \dfrac{\partial\rho_1}{\partial\phi_2}\tan\theta_1 & 0 \end{pmatrix}, \tag{A.1}$$

where $\rho_1 = \sqrt{(x+d/2)^2+y^2}$ and

$$\frac{\partial\rho_1}{\partial\phi_i} = \frac{1}{\rho_1}\left(\frac{\partial x}{\partial\phi_i}(x+d/2)+\frac{\partial y}{\partial\phi_i}y\right), \quad i=1,2. \tag{A.2}$$

Instead of taking the derivative of h with respect to $\mathbf{p}$ to apply the chain rule, we can directly take the derivative of (27), (28). We take the derivative with respect to $\mathbf{v}$ in which the equations are linear. It is easy to see that

$$\frac{\partial t_1 \circ h}{\partial \mathbf{v}} = -\frac{T}{\sin(\phi_2-\phi_1)}\begin{pmatrix}\cos\phi_1\\ \sin\phi_1\\ \tan\theta_1\end{pmatrix}\begin{pmatrix}\sin\phi_2 & -\cos\phi_2 & 0\end{pmatrix} \tag{A.3}$$

which gives everything necessary to calculate the covariance according to (14).

A.2. Solving the ambiguity in ρ_1

To solve the ambiguity in (35) we see that

$$q = \frac{\tan\theta_2}{\tan\theta_1} = \frac{\rho_1}{\rho_2} \tag{A.4}$$

is the ratio of the two ground ranges. This implies intersecting two circles with fixed centers and their radii obeying a certain ratio. The set of all possible solutions of this is generally a circle. We differentiate two cases.

(i) For $q = 1$ the radii are equal and the set of all points is a line, that is, a degenerate circle; it is the perpendicular bisector of the line connecting the centers.
(ii) For $q \neq 1$ all solutions are on a circle surrounding, but not necessarily centered around the center of the smaller circle.

From this we figure that given ϕ_1 we intersect a ray originating from the center of circle one with the above solution. In case of $q = 1$ the ray has to intersect the bisector, which it will only for $\phi_1 \in [-\pi/2, \pi/2]$ which we can see in (34). For $q < 1$ the above solution is a circle surrounding the origin of the ray, therefore they intersect excatly once. (One of the solutions for ρ_1 in (35) will be negative, which can be interpreted that including negative ρ_1 we change the ray for a line which would intersect twice.) For $q > 1$ we intersect the ray with a circle not surrounding the origin of the ray, which can lead to two solutions, just one or none, depending on the geometry. We observe that the second azimuth ϕ_2 is π for the smallest possible ground range ρ_1 and strictly decreases to zero as ρ_1 increases. Now we only have to show that $\phi_2 = \pi/2$ is the singular solution, as it is the devider between the solutions with positive or negative square root in (35). If $\phi_2 = \pi/2$, then it follows that

$$x = \rho_2\cos\phi_2 + d/2 = d/2 \iff \rho_1\cos\phi_1 = d. \tag{A.5}$$

Next we insert

$$\rho_1 = d\left(-\frac{q^2\cos\phi_1}{1-q^2}\right) \tag{A.6}$$

into the above equation:

$$\begin{aligned} -d\frac{q^2\cos^2\phi_1}{1-q^2} &= -d\frac{\rho_1^2\cos^2\phi_1}{\rho_2^2-\rho_1^2} \\ &= -d\frac{(x+d/2)^2}{(x-d/2)^2-(x+d/2)^2} \\ &= \frac{(x+d/2)^2}{2x} = d, \end{aligned} \tag{A.7}$$

which for $x \neq 0$ leads to

$$\left(x+\frac{d}{2}\right)^2 - 2dx = x^2 - dx + \frac{d^2}{4} = \left(x-\frac{d}{2}\right)^2 = 0. \quad \text{(A.8)}$$

A.3. Derivatives for one azimuth, two elevation

We will calculate the derivatives $\partial t_3/(\partial \mathbf{z}-\mathbf{w})$ and $\partial t_3 \circ h/\partial \mathbf{x}$. We start from (30), which all depend on ρ_1 from (33). The derivatives with respect to $\mathbf{z}-\mathbf{w}$ are given in

$$\frac{\partial t_3}{\partial \mathbf{z}-\mathbf{w}} = \begin{pmatrix} \frac{\partial \rho_1}{\partial \phi_1}\cos\phi_1 - \rho_1\sin\phi_1 & \frac{\partial \rho_1}{\partial \theta_1}\cos\phi_1 & 0 & \frac{\partial \rho_1}{\partial \theta_2}\cos\phi_1 \\ \frac{\partial \rho_1}{\partial \phi_1}\sin\phi_1 + \rho_1\cos\phi_1 & \frac{\partial \rho_1}{\partial \theta_1}\sin\phi_1 & 0 & \frac{\partial \rho_1}{\partial \theta_2}\sin\phi_1 \\ \frac{\partial \rho_1}{\partial \phi_1}\tan\theta_1 & \frac{\partial \rho_1}{\partial \theta_1}\tan\theta_1 + \frac{\rho_1}{\cos^2\theta_1} & 0 & \frac{\partial \rho_1}{\partial \theta_2}\tan\theta_1 \end{pmatrix}, \quad \text{(A.9)}$$

with the following partial derivatives

$$\begin{aligned} \frac{\partial \rho_1}{\partial \phi_1} &= \frac{dq^2\sin\phi_1\rho_1}{dq^2\cos\phi_1 + (1-q^2)\rho_1}, \\ \frac{\partial \rho_1}{\partial \theta_i} &= \frac{\rho_1^2 - 2d\cos\phi_1\rho_1 + d^2}{dq^2\cos\phi_1 + (1-q^2)\rho_1} q\frac{\partial q}{\partial \theta_i} \quad i = 1,2, \\ \frac{\partial q}{\partial \theta_1} &= -\frac{\tan\theta_2}{\sin^2\theta_1}, \qquad \frac{\partial q}{\partial \theta_2} = \frac{1}{\tan\theta_1\cos^2\theta_2}. \end{aligned} \quad \text{(A.10)}$$

To differentiate $t_3 \circ h$ in $\mathbf{v}$ we will linearize (32) around $T = 0$. We find

$$\frac{\partial \rho_1}{\partial T} = -\frac{\rho_1\cot\theta_1\dot{z} - q^2(\rho_1\cos\phi_1 - d)\dot{x} - q^2\rho_1\sin\phi_1\dot{y}}{\rho_1(1-q^2) + (q^2\cos\phi_1 d)} \quad \text{(A.11)}$$

which is linear in $\dot{x}$, $\dot{y}$, and $\dot{z}$. For small T we can approximate ρ_1 by $\rho_1 = \rho_1|_{T=0} + T(\partial\rho_1/\partial T)$. Defining

$$N = \rho_1(1-q^2) + (q^2\cos\phi_1 d) \quad \text{(A.12)}$$

and using (30), the result is

$$\frac{\partial t_3 \circ h}{\partial \mathbf{v}} = -T\begin{pmatrix}\cos\phi_1 \\ \sin\phi_1 \\ \tan\theta_1\end{pmatrix}\left(-\frac{q^2(\rho_0\cos\phi_1 - d)}{N} \quad -\frac{q^2\rho_0\sin\phi_1}{N} \quad \frac{\rho_0\cot\theta_1}{N}\right), \quad \text{(A.13)}$$

where $\rho_0 = \rho_{1|_{T=0}}$ is the solution to (33).

B. RANGE AND AZIMUTH SCENARIO

B.1. Derivatives for two azimuth, one range

To calculate the covariance matrix, we already have most derivatives from the previous section, but still need to take the derivative of (37). The result for $\partial t_1/(\partial \mathbf{z}-\mathbf{w})$ is

$$\frac{\partial t_1}{\partial \mathbf{z}-\mathbf{w}} = \begin{pmatrix} d\frac{\sin\phi_2\cos\phi_2}{\sin^2(\phi_2-\phi_1)} & 0 & -d\frac{\sin\phi_1\cos\phi_1}{\sin^2(\phi_2-\phi_1)} & 0 \\ d\frac{\sin^2(\phi_2)}{\sin^2(\phi_2-\phi_1)} & 0 & -d\frac{\sin^2(\phi_1)}{\sin^2(\phi_2-\phi_1)} & 0 \\ -\frac{d^2}{z}\frac{\sin^2(\phi_2)\cos(\phi_2-\phi_1)}{\sin^3(\phi_2-\phi_1)} & \frac{r_1}{z} & -\frac{d^2}{z}\frac{\sin\phi_1\sin\phi_2}{\sin^3(\phi_2-\phi_1)} & 0 \end{pmatrix}, \quad \text{(B.1)}$$

where for z we have to use our estimate. For $\partial t_1 \circ h/\partial \mathbf{v}$,

$$\frac{\partial t_1 \circ h}{\partial \mathbf{v}} = \frac{T}{\sin(\phi_2-\phi_1)}\begin{pmatrix}\cos\phi_1 \\ \sin\phi_1 \\ -\frac{d\sin\phi_2}{z\sin(\phi_2-\phi_1)}\end{pmatrix}\begin{pmatrix}\sin\phi_2 & -\cos\phi_2 & 0\end{pmatrix}. \quad \text{(B.2)}$$

B.2. Derivatives for one azimutn, two range

For the $\{r_1, r_2, \phi_1\}$ case the derivatives to calculate the covariance are

$$\frac{\partial t_3}{\partial \mathbf{z}-\mathbf{w}} = \begin{pmatrix} 0 & \frac{r_1}{d} & 0 & -\frac{r_2}{d} \\ \frac{\rho_1}{\cos\phi_1} & \frac{r_1}{d}\tan\phi_1 & 0 & -\frac{r_2}{d}\tan\phi_1 \\ -\frac{\rho_1^2\tan\phi_1}{z} & \frac{r_1}{z}\left(1-\frac{\rho_1}{d\cos\phi_1}\right) & 0 & \frac{r_2}{z}\frac{\rho_1}{d\cos\phi_1} \end{pmatrix}$$

$$\frac{\partial t_3 \circ h}{\partial \mathbf{v}} = \frac{T}{2d}\begin{pmatrix}1 \\ \tan\phi_1 \\ -\frac{x+d/2}{z}(1+\tan^2\phi_1)\end{pmatrix}\begin{pmatrix} d & -2x & -2y & -2z \end{pmatrix} \quad \text{(B.3)}$$

where for ρ and x, y, z the estimated values have to be used.

ACKNOWLEDGMENTS

The authors would like to thank Dr. Peter Willett of the Department of Electrical and Computer Engineering, University of Connecticut, and Dr. Klaus Becker of the Sensor Networks and Data Fusion Group, FGAN e.V., for the helpful

discussions, comments, and suggestions during the research and writing of this paper. C. R. Berger is supported by the Office of Naval Research. This paper was presented in part at the FUSION, Quèbec, Canada, July 2007 [11].

REFERENCES

[1] S. C. Nardone and V. J. Aidala, "Observability criteria for bearings-only target motion analysis," *IEEE Transactions on Aerospace and Electronic Systems*, vol. 17, no. 2, pp. 162–166, 1981.

[2] K. Becker, "Target motion analysis aus Winkelmessungen: parametrischeStudie in drei Dimensionen," FGAN, Wachtberg-Werthoven, FKIE Bericht 12, 2000.

[3] Y. Bar-Shalom, X. R. Li, and T. Kirubarajan, *Estimation with Application to Tracking and Navigation*, John Wiley & Sons, New York, NY, USA, 2001.

[4] S. C. Nardone and M. L. Graham, "A closed-form solution to bearings-only target motion analysis," *IEEE Journal of Oceanic Engineering*, vol. 22, no. 1, pp. 168–178, 1997.

[5] G. van Keuk, "Ein Basisalgorithmus für die räumliche Triangulation," FGAN, Wachtberg-Werthoven, FFM Bericht 418, 1991.

[6] V. Aidala, "Kalman filter behavior in bearings-only tracking applications," *IEEE Transactions on Aerospace and Electronic Systems*, vol. 15, no. 1, pp. 29–39, 1979.

[7] T. Kirubarajan, Y. Bar-Shalom, and D. Lerro, "Bearings-only tracking of maneuvering targets using a batch-recursive estimator," *IEEE Transactions on Aerospace and Electronic Systems*, vol. 37, no. 3, pp. 770–780, 2001.

[8] W. Koch, J. Koller, and M. Ulmke, "Ground target tracking and road map extraction," *ISPRS Journal of Photogrammetry & Remote Sensing*, vol. 61, no. 3-4, pp. 197–208, 2006.

[9] S. J. Julier and J. K. Uhlmann, "Unscented filtering and nonlinear estimation," *Proceedings of the IEEE*, vol. 92, no. 3, pp. 401–422, 2004.

[10] H. van Trees, *Detection, Estimation, and Modulation Theory*, John Wiley & Sons, New York, NY, USA, 1st edition, 1986.

[11] C. R. Berger, M. Daun, and W. Koch, "Track initialization from incomplete measurements," in *Proceedings of the 10th International Conference on Information Fusion (FUSION '07)*, Quèbec, Canada, July 2007.